Spectroscopic study and enhanced thermostability of combustion-derived BaMgAl10O17:Eu2+ blue phosphors for solid-state lighting

Nathalie Pradal, Audrey Potdevin, Geneviève Chadeyron, Pierre Bonville, Bruno Caillier, Rachid Mahiou

▶ **To cite this version:**

Nathalie Pradal, Audrey Potdevin, Geneviève Chadeyron, Pierre Bonville, Bruno Caillier, et al.. Spectroscopic study and enhanced thermostability of combustion-derived BaMgAl10O17:Eu2+ blue phosphors for solid-state lighting. Optical Materials, 2017, 64, pp.334 - 344. 10.1016/j.optmat.2016.12.031 . cea-01507459

HAL Id: cea-01507459
https://cea.hal.science/cea-01507459v1

Submitted on 13 Apr 2017

HAL is a multi-disciplinary open access archive for the deposit and dissemination of scientific research documents, whether they are published or not. The documents may come from teaching and research institutions in France or abroad, or from public or private research centers.

L'archive ouverte pluridisciplinaire **HAL**, est destinée au dépôt et à la diffusion de documents scientifiques de niveau recherche, publiés ou non, émanant des établissements d'enseignement et de recherche français ou étrangers, des laboratoires publics ou privés.

Optical Materials 64 (2017) 334–344

Contents lists available at ScienceDirect

Optical Materials

journal homepage: www.elsevier.com/locate/optmat

Spectroscopic study and enhanced thermostability of combustion-derived $BaMgAl_{10}O_{17}:Eu^{2+}$ blue phosphors for solid-state lighting

Nathalie Pradal [a, b], Audrey Potdevin [a, b, *], Geneviève Chadeyron [a, b, **], Pierre Bonville [d], Bruno Caillier [e], Rachid Mahiou [b, c]

[a] Université Clermont Auvergne, Sigma-Clermont, Institut de Chimie de Clermont-Ferrand, BP 10448, F-63000 Clermont-Ferrand, France
[b] CNRS, UMR 6296, ICCF, F-63178 Aubiere, France
[c] Université Clermont Auvergne, Université Blaise Pascal, Institut de Chimie de Clermont-Ferrand, BP 10448, F-63000 Clermont-Ferrand, France
[d] CEA, Centre de Saclay, DSM/Service de Physique de l'Etat Condensé, F-91191 Gif-sur-Yvette, France
[e] Laboratoire Diagnostics des Plasmas Hors équilibre - DPHE, Université de Toulouse, INU Champollion, DPHE, Place de Verdun, F-81012 Albi, France

ARTICLE INFO

Article history:
Received 8 December 2016
Received in revised form
16 December 2016
Accepted 19 December 2016
Available online 5 January 2017

Keywords:
LEDs
Combustion derived BAM:Eu
Solid-state lighting
Thermal stability

ABSTRACT

Blue-emitting $BaMgAl_{10}O_{17}:Eu^{2+}$ (BAM:Eu), suitable for applications in a next generation of Hg-free lamps based on UV LEDs, was prepared by a microwave induced solution combustion synthesis, using urea as combustion fuel and nitrates as oxidizers. Purity control of the as-synthesized blue phosphor was undertaken by a washing step followed by a reduction one. Structural and morphological properties of the outcoming phosphors have been considered. Synthesis process allows producing a well-crystallized and nanostructured BAM phase within only few minutes. The influence of reduction treatment on the relative amounts of Eu^{2+}/Eu^{3+} in our samples has been investigated through an original study by magnetization and Mössbauer spectroscopy. Furthermore, a complete optical study has been carried out and allowed us to determine the europium localization in the three possible sites in BAM matrix. The percentage of Eu^{2+} increased twofold after the reduction treatment, entailing an increase in the luminescence efficiency upon UV excitation. Finally, temperature-dependent luminescence of combustion-derived powders has been studied till 170 °C and compared to that of commercial BAM:Eu. MISCS-derived phosphors present a higher thermal stability than commercial one: whereas the emission efficiency of this last was reduced by 64%, the one of combustion-derived BAM:Eu experienced an only 12% decline. Furthermore, while commercial BAM suffered from a severe blue-shift with increasing temperature, our phosphors keep its color quality with a good stability of the photometric parameters.
© 2016 Elsevier B.V. All rights reserved.

1. Introduction

Nowadays, phosphor-converted white light-emitting diodes (pc-WLEDs) are considered as the most promising eco-friendly light sources, mercury free and more efficient than conventional lighting devices (incandescent bulbs and compact fluorescent tubes) since LEDs present superior lifetime, efficiency and reliability [1–5]. Combining near ultraviolet (near UV - 350 nm $\leq \lambda_{em} \leq$ 400 nm) diode chips with a mixture of red, green and blue phosphors to produce white light appears as a promising alternative with several advantages compared to current commercial WLEDs using a 460 nm blue GaN LED chip covered by a $Y_3Al_5O_{12}:Ce^{3+}$ (YAG:Ce) yellowish phosphor coating. Indeed, this latter suffers from serious drawbacks such as low color-rendering index (CRI) due to relatively weak emission in the red spectral region and low stability of color temperature [2,6]. To overcome these drawbacks that slow down an effective penetration of general public lighting market, the new "UV LED/phosphors" associations seem very encouraging since they give access to a wide gamut of colors and controlled CRI. Their versatility is due to the possibility of tuning both phosphors formulations and proportions [7], numerous phosphors being suitable with the UV excitation wavelengths used in this kind of devices. Since chips generate heat [7] (up to 400–450 K at junction), in particular in high-power LEDs, these phosphors are required to provide excellent thermally stable

* Corresponding author. Université Clermont Auvergne, Sigma-Clermont, Institut de Chimie de Clermont-Ferrand, BP 10448, F-63000 Clermont-Ferrand, France.
** Corresponding author. Université Clermont Auvergne, Sigma-Clermont, Institut de Chimie de Clermont-Ferrand, BP 10448, F-63000 Clermont-Ferrand, France.
E-mail addresses: audrey.potdevin@sigma-clermont.fr (A. Potdevin), Genevieve.chadeyron@sigma-clermont.fr (G. Chadeyron).

http://dx.doi.org/10.1016/j.optmat.2016.12.031
0925-3467/© 2016 Elsevier B.V. All rights reserved.

luminescence. Using efficient phosphors, characterized by not only suitable luminescence features (emission and excitation profiles) but also by thermal stability of luminescence and short emission decay is thus of paramount importance to obtain long-lasting effective pc-WLEDs [7–11].

Among these phosphors, $BaMgAl_{10}O_{17}:Eu^{2+}$ phosphor (BAM:Eu) appears as a promising blue phosphor for near-UV LEDs based lighting devices [7,12]. During last decades, it has attracted considerable attention since it has been widely used for modern advanced devices such as plasma display panels (PDPs) and mercury-free lamps [13–15]. Indeed, it is known for possessing high luminance efficiency and good color purity under both vacuum ultraviolet (VUV) and ultraviolet (UV) excitations. But it is also famous to suffer from thermal and photo degradation entailing changes in its color purity and decrease in its luminescence efficiency both during the baking process while manufacturing (thermal damage) or during operation i.e. UV or VUV irradiation damage. These behaviors have already been studied in some papers that revealed this thermal degradation is related to different concomitant phenomena including oxidation of Eu ions [16–19]. To the best of our knowledge, temperature-dependent luminescence of $BAM:Eu^{2+}$ upon near UV radiation has been scarcely studied [20–22] and mainly in comparison with other phosphors. However, thermostability of other Eu^{2+}-doped phosphors for solid-state lighting upon blue or UV radiation has been recently studied [20–30]. These works have revealed both irreversible thermal degradation and reversible thermal quenching. These phenomena seem related both to the host matrix and its synthesis procedure. To improve thermal stability of BAM:Eu, we have chosen to synthesize it by an alternative preparation technique: the microwave-induced solution combustion synthesis (MISCS) [31,32].

Conventionally, BAM:Eu phosphor is obtained *via* an energy consuming solid-state reaction process requiring a several hour-heating treatment at high temperatures (above 1300 °C) leading to large size range and irregular shapes, inappropriate for the devices foreseen [33–35]. Ball milling is often used after heat treatment to address these problems but it results in defects on the particles, surface contamination and crystal structure damage, leading to reduced phosphor luminance efficiency and stability. MISCS is a hopeful process in terms of energy saving and equipment and can produce a large variety of oxides within a short duration from cheap precursors (nitrates and an organic fuel) [36,37]. Without further calcination, it leads to well-crystallized powders characterized by small grain sizes with a narrow size distribution easily dispersible in common solvents or polymers [38]. This feature allows, for instance, shaping the materials as homogeneous films suitable for LEDs based lighting devices. This is particularly interesting since the current trend in the field of lighting devices is to develop large luminescent areas. Furthermore, it has been notably reported [39,40] that the phosphors prepared *via* wet chemical processes exhibited stronger emission intensity and higher thermal stability than the samples derived from solid-state reaction.

In this work, structural, morphological and optical properties of MISCS-derived $BaMgAl_{10}O_{17}:Eu^{2+}$ are presented. As-prepared phosphor have also been submitted to a reduction step since it could be assumed that a residual part of trivalent europium, originating from the synthesis precursors, still remained in the powder after the synthesis. The influence of this reduction step on powders optical properties have been studied and correlated to the relative fractions of divalent and trivalent europium by photoluminescence and both magnetization and Mössbauer spectroscopy respectively. The reductive annealing treatment leads to increase the proportion of Eu^{2+} and so on luminescence efficiency. Temperature-dependent emission spectra of these combustion derived phosphors have been studied upon 365 nm excitation (near UV LED) from room temperature till 170 °C. The evolution of emission spectra with time at 170 °C was also examined. Commercial BAM was comparatively studied by Mossbaüer spectroscopy and photoluminescence. Quantum yields of both kinds of phosphors have been measured before and after thermal and photo-degradations.

2. Experimental section

2.1. Preparation of Eu^{2+}-doped $BaMgAl_{10}O_{17}$

$Ba_{0.9}Eu_{0.1}MgAl_{10}O_{17}$ powders were prepared by a microwave-assisted combustion synthesis [32] using $CO(NH_2)_2$ (Sigma-Aldrich, purity 99.5%) as fuel and $Ba(NO_3)_2$ (Sigma-Aldrich, purity 99+%), $Mg(NO_3)_2{\cdot}6H_2O$ (Acros organics, purity 99+%), $Al(NO_3)_3{\cdot}9H_2O$ (Sigma-Aldrich, purity 99.997+%) and $Eu(NO_3)_3{\cdot}5H_2O$ (Sigma-Aldrich, purity 99.9+%) as metallic precursors. Metal nitrates were weighed stoichiometrically, dissolved in distilled water in a beaker and stirred in order to obtain a clear solution. Then, urea was added with the optimized fuel to oxidizer molar ratios (f/o). The theoretical (stoichiometric) molar ratio of urea to nitrate $(f/o)_{th}$ is in this case 2.36:1, based on the total oxidizing and reducing valences of the oxidizer and the fuel [1]. The beaker containing the solution (fuel + nitrates) was placed into a domestic microwave oven which always operated at its maximum power setting (900 W). The solution boiled, underwent dehydration followed by nitrates and urea decomposition, leading to the formation of a large amount of gases (CO_2, N_2 and H_2O) and then burst into a white flame. The whole process, very exothermic, spent a few minutes and resulted into a foamy white powder, composed of blue and red parts when exposed to UV radiation. Since the part intended as phosphors for lighting devices is the blue one, this latter has been isolated before being characterized. The duration of heating, the power level and the solution concentrations were optimized following a number of trials and were found to give rise to highly reproducible results concerning structural, morphological and optical properties of as-obtained phosphors. A previous work [32] allowed us to determine that the optimal fuel to oxidizer molar ratio leading to the highest proportion of well crystallized blue phosphor corresponds to the stoichiometric $(f/o)_{th}$ increased by a factor of three. In these conditions, the red part represents less than 10w% of the whole as-synthesized powder. Since the as-synthesized blue part contains a little fraction of $BaAl_2O_4$ (as seen later in the XRD study), an additional washing step has been carried out to purify BAM phase and theoretically improve its optical performances. Thus, this powder emitting in the blue range was washed several times with acidic distilled water (pH ≈ 2 by the addition of a concentrate HNO_3 solution). Then, a post-heating treatment in a reducing atmosphere (H_2/N_2 5%/95%) at 1300 °C for 150 min, with a heating rate of 5 °C.min^{-1}, has been carried out in order to enhance the quantity of Eu^{2+} responsible for the desired luminescence properties.

For comparison, we also studied a commercial BAM:Eu powder provided by Rhodia-Solvay (reference CRT013).

2.2. Characterization techniques

XRD patterns were recorded on a Philips Xpert Pro diffractometer operating with the Cu-Kα radiation (λ = 1,5406 Å). CaRIne Crystallography v3.1 software was used to simulate XRD pattern from the crystallographic data and to schematize the spatial BAM:Eu structure [41,42]. An attenuated total reflection (ATR) accessory installed on a Nicolet FTIR spectrometer was used to record ATR spectra. Micrographs were investigated by means of a ZEISS Supra 55VP Scanning Electron Microscope (SEM) operating in

high vacuum at 3 kV, using secondary electron detector (Everhart-Thornley detector). Specimens were prepared by sticking powder onto the surface of an adhesive carbon film.

The isothermal magnetization measurements were performed using a CRYOGENIC Vibrating Sample Magnetometer with a maximum field of 14 T, operating between 1.7 K and 300 K. The Mössbauer spectra on the isotope ^{151}Eu were performed at 77 K in a standard He cryostat, using a Sm^*F_3 γ-ray source and a constant acceleration electromagnetic drive.

Room temperature emission and excitation features of BAM:Eu powders were measured using the C9920-02G PL-QY measurement system from Hamamatsu. The setup comprises a 150 W monochromatized Xe lamp, an integrating sphere (Spectralon® Coating, Ø = 3.3 inch) and a high sensitivity CCD spectrometer for detecting the whole spectral luminescence. It has also been used to measure internal quantum yields (QY) and Absorbances. By multiplying these two data, we obtained absolute QY. Thermal stability has been studied using a 365 nm LED as an excitation source and a CCD camera cooled by liquid nitrogen as a detector. Samples were placed a home-made [43] copper holder heated by a thermocoax wire connected to a temperature controller. At a given temperature, emission spectra were automatically recorded at regular intervals.

To obtain the decay time, the pellet sample is first illuminated with a 365 ± 10 nm LED (LED365W from Thorlabs) at 400 Hz frequency (2500μs period). Then, the light is collected with a fast Intensified Camera (ICCD Princeton Imax). The 5000 accumulations on CCD mode, the controlled size gate from 4ns to 5μs and the intensification of the camera allow us a very low noise on the 3 log-decades decay.

3. Results and discussion

3.1. Structure and phase characterization

BAM:Eu crystallization was analyzed by means of XRD. Fig. 1 exhibits a comparison of XRD patterns obtained for blue phosphor at each step of the process: at the end of the combustion synthesis (called “before acid-wash”, Fig. 1b), after the washing step (called “after acid-wash”, Fig. 1c) and after the post-heating reduction treatment (called “after reduction”, Fig. 1d). This figure also presents the simulated XRD pattern for BAM:Eu^{2+} (Fig. 1a) plotted from the crystallographic data [41,42]. The X-Ray pattern obtained for powder “before acid-wash” (Fig. 1b) reveals that the blue powder corresponds to nearly pure $BaMgAl_{10}O_{17}$ phase with a very little fraction of $BaAl_2O_4$ phase (identified by arrows). As a consequence, an acid-washing has been carried out in order to remove the unwanted $BaAl_2O_4$ phase (mainly identified by the peak localized at 28° in 2θ). All the diffraction peaks observed on the resulting pattern (Fig. 1c) are assigned to the BAM structure. An acid-leaching treatment leads to the disappearance of $BaAl_2O_4$ phase and results in pure BAM phase.

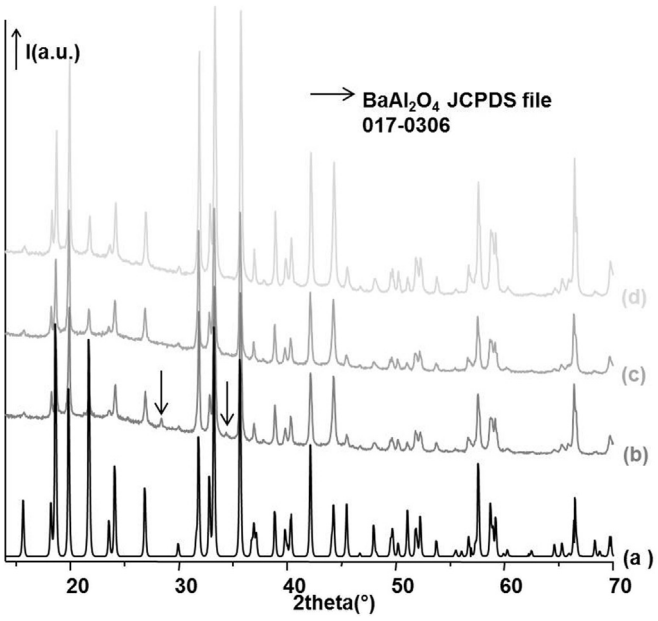

Fig. 1. XRD patterns of blue phosphors (b) before, (c) after acid-wash, (d) after reduction and (a) the simulated pattern for BAM:Eu.

Concerning the blue phosphor after the reduction treatment (Fig. 1d), once again all the diffraction peaks correspond to BAM phase but it can be noticed a more significant crystallization with a stronger intensity of diffraction peaks. Furthermore, in first approximation, the average crystallites size has been determined from the full-width at half-maximum (FWHM) of the diffraction peaks using Scherrer's equation [44].

$$< D > = k \cdot \lambda / \beta \cdot \cos\theta \quad (1)$$

where D is the mean particle size, k is a geometric factor (here, k = 0.9), λ is the X-ray wavelength, and β is the corrected half-width of the diffraction peak located at about 26.9° (2θ). Estimated from the Formula (1), whatever the step of the process (as-prepared, after washing and after reduction treatment), the average crystallites size of the combustion-derived BAM particles are about 40 nm. The different purification stages do not lead to variation in crystallites size.

FT-IR spectrum of $BaMgAl_{10}O_{17}$:Eu^{2+} blue powder after acid-wash is presented in Fig. 2. Acid-washing and reduction treatment do not affect the IR results. Bands ranging from 1100 to 400 cm^{-1} arise from the metal-oxygen (M-O) groups. No band over 1100 cm^{-1} are recorded testifying to the absence of organic residue.

BAM:Eu^{2+} has a β-alumina structure and belongs to the $P6_3/mmc$ space group. This structure consists of a spinel block composed of aluminum, magnesium and oxygen ($MgAl_{10}O_{16}$) organized in AlO_4 tetrahedrons and AlO_6 octahedrons, so there are two sites for Al^{3+} ions. Mg^{2+} ions occupy one Al site. Two spinel layers are connected by a conduction layer (BaO) where Ba^{2+} ions are substituted by Eu^{2+} [39]. The crystal structure of $BaMgAl_{10}O_{17}$ is

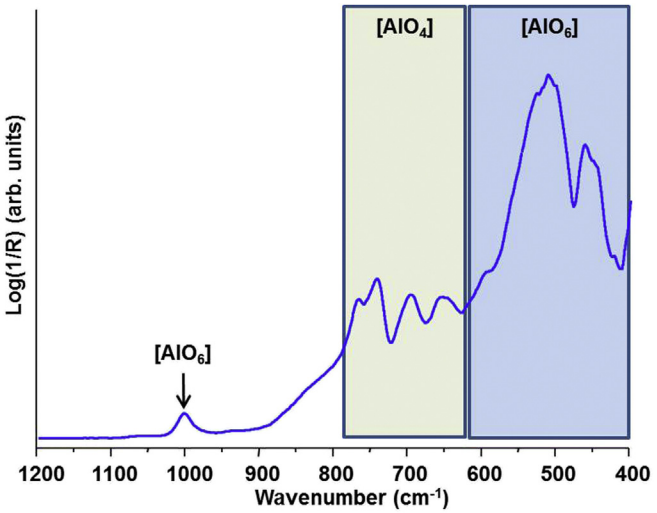

Fig. 2. FTIR spectrum of blue powder after acid-wash.

depicted on Fig. S1 [41]. IR absorption bands located at 1000 cm^{-1} and from 595 to 445 cm^{-1} are attributed to the absorption of [AlO_6] octahedrons. The absorption bands located from 765 to 650 cm^{-1} can be ascribed to [AlO_4] tetrahedrons [45].

3.2. Morphological study

Fig. 3 shows the SEM images of BAM:Eu blue powders at each step of the process (Fig. 3a–c). Whatever blue emitting powder obtained from MISCS, SEM images show that particles present a specific plate-like nanostructure shape. The platelets thickness varies from 40 to 80 nm and their diagonal from 200 to 500 nm. The different purification stages did not lead to any variation in morphology. For comparison, SEM image of the commercial BAM:Eu powder is shown in Fig. 3d. As seen, it presents micrometric, very smooth and heterogeneous grains with platelet shape together with some micronic aggregates. It is very different from powders prepared by MISCS which are nanostructured and homogeneous. As a result, these particles can be easily dispersed in a medium, for instance to elaborate homogeneous luminescent coatings from phosphors in suspension [38] whereas particles with a very dense and large size distribution cannot.

3.3. Determination of the relative fractions of divalent and trivalent europium

Divalent europium is responsible for the desired blue luminescence but it can be assumed that a residual part of trivalent europium, originating from the synthesis precursor ($Eu(NO_3)_3 \cdot 5H_2O$), still remains in the powder after the synthesis.

Consequently, a study by magnetization (Fig. 4) was made to evaluate the percentage of divalent europium relative to total europium in our samples and to determine the influence of purification steps (acid-washing and reduction treatment) on this ratio. Both Eu valencies are paramagnetic, but divalent europium has a large moment of $7\mu_B$, its isothermal magnetization obeying a Brillouin function, whereas trivalent europium is a Van-Vleck ion with weak temperature independent susceptibility [46]. So it is rather

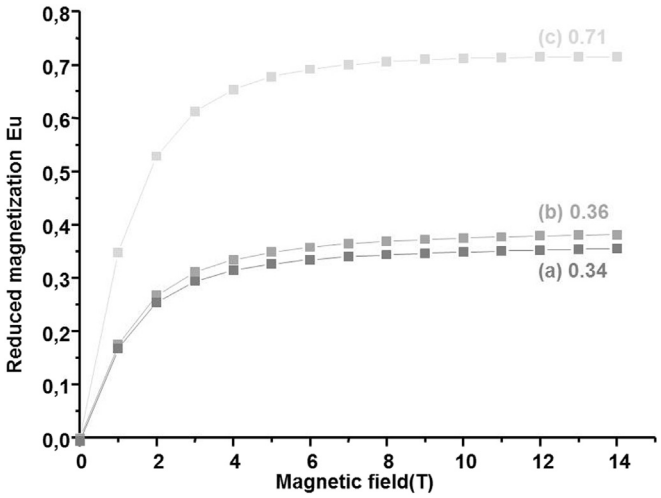

Fig. 4. Reduced magnetization of blue phosphors (a) before, (b) after acid-wash and (c) after reduction.

easy to obtain the fraction of Eu^{2+} from a magnetization curve provided the total Eu fraction in the sample is known. As seen in Fig. 5, the acid-washing did not lead to a modification of the percentage of divalent europium: it reaches around 35% at the end of the synthesis and after the elimination of $BaAl_2O_4$ phase. Synthesis conditions of BAM:Eu are not reductive enough to end at the complete reduction of Eu^{3+} into Eu^{2+}. However, the reduction treatment allowed to increase this percentage by a factor of two (71%), having significant consequences on optical properties (see luminescence properties).

In order to confirm these promising results, the same kind of study has been realized by Mössbauer spectroscopy (Fig. 5); only results obtained on purified powders are presented here. It is rather easy to distinguish between the two valences in the Mössbauer spectra since the Eu^{3+} component yields a narrow line centered at an energy-equivalent velocity close to 0 mm s^{-1}, while the Eu^{2+}

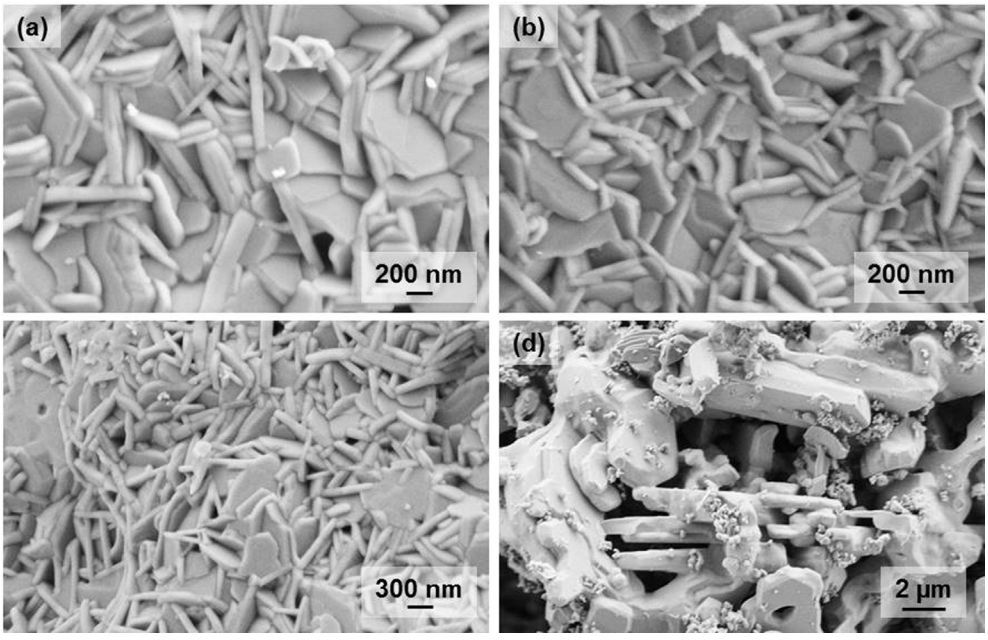

Fig. 3. SEM images of MISCS blue phosphors (a) before, (b) after acid-wash, (c) after reduction and (d) a commercial BAM:Eu powder (Rhodia-Solvay).

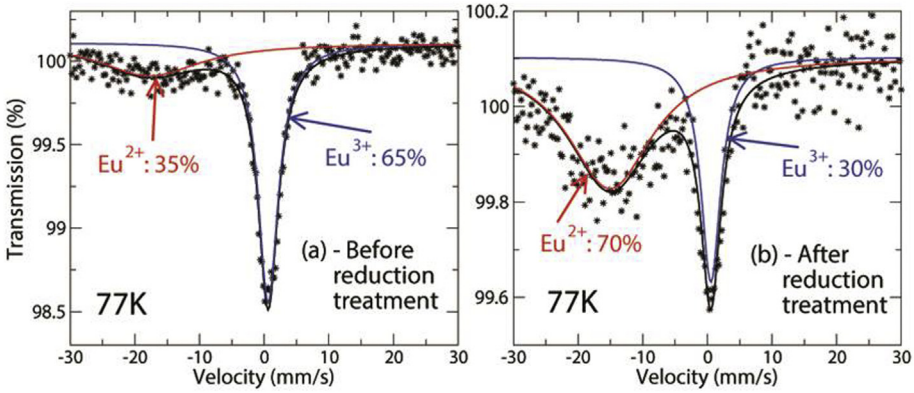

Fig. 5. ^{151}Eu Mössbauer absorption spectra of blue phosphors (a) after acid-wash and (b) after reduction.

component is broad and centered near a velocity of −12 mm s^{-1} [47,48].

The Mössbauer absorption spectrum of acid-washed $Ba_{0.9}Eu_{0.1}MgAl_{10}O_{17}$ has a dominant component of trivalent europium (Fig. 5a). The presence of a divalent europium component was detected by the quite clear asymmetry of the spectrum in the negative region of the velocity, indicating that a broad Eu^{2+} subspectrum is present. Previous studies using Mössbauer spectroscopy for characterizing BAM:Eu have correlated this asymmetric signal for Eu^{2+} to the different sites occupied by these ions, with each site represented by a quadrupolar pattern, characteristic of the $7/2^+ \rightarrow 5/2^+$ spin sequence [48,49]. We will discuss about these multiple sites in the part concerning luminescence properties, based instead on PL spectra profiles. The purpose of using Mössbauer spectroscopy in this work was to determine the relative fractions of Eu^{2+} and Eu^{3+} ions. Fitting the two components observed in Fig. 6 to Lorentzian-shaped bands reveals that there remains an important percentage of Eu^{3+} in washed blue phosphor (65%). After reduction treatment, the trend is reversed (Fig. 5b): the spectrum exhibits a broad line with an isomer shift (IS) of −15 mm s^{-1} assigned to Eu^{2+} which is the dominant component: the percentage of divalent europium has increased by a factor of two to reach 70%. Results obtained by Mössbauer spectroscopy are in good agreement with those derived from magnetization technique.

Commercial BAM was also analyzed by Mössbauer spectroscopy (Fig. S2). It revealed a percentage of divalent europium of 80% which is probably due to a reduction treatment at a temperature higher than ours (1300 °C). This assumption is consistent with the SEM image presented in Fig. 3d showing facetted microparticles.

3.4. Room-temperature photoluminescence

Afterward, all the presented results concern pure BAM:Eu phosphor: samples are called “before” and “after reduction treatment” (note: in this section, the sample called “before reduction treatment” corresponds to that called “after acid-wash” in the other parts of the manuscript).

Photoluminescence quantum yields of both purified $Ba_{0.9}Eu_{0.1}MgAl_{10}O_{17}$ powders have been measured tuning the excitation in the 250–450 nm range and are presented in Fig. 6a. It can be observed that quantum yield is higher for reduced powder, whatever the excitation wavelength which is concordant with previous Mössbauer and magnetization results: a higher quantity of Eu^{2+} ions leads to a better luminescence efficiency.

These spectra show the same overall shape: the absorption bands correspond to characteristic Eu^{2+} electronic transitions connecting the ground state to the split crystal field 5d levels [37]. According to previous works [48,50–52], it has been demonstrated that in BAM host lattice, europium substituted for barium ions and can have three possible locations named Beevers-Ross (BR), anti-Beevers-Ross (a-BR) and middle-oxygen (mO). They have different local symmetry leading to different divalent europium ions optical behavior. As a consequence, BAM:Eu total excitation spectrum is expected to reflect the contribution of individual excitation spectra of Eu^{2+} ions located on the possible sites of substitution in the matrix [53].

Eu^{2+} ions localized in sites with different local symmetry have not exactly the same excitation spectral response due to the own 5d level energy location and splitting induced by the local crystal field. According to the literature [53], BAM:Eu excitation spectra can be fitted into five Gaussian bands in the 250–450 nm wavelength spectral range (40000-22222 cm^{-1} in energy). Then, such a refinement has been applied to both recorded excitation spectra: results appear on Fig. 6b and c. Moreover, Table 1 summarizes the results and gives a comparison with the literature [53].

It gathers peak location, area of individual contributions and their assignments in terms of substitutions sites. Excitation spectra (Fig. 6b and c) can be fitted by five bands centered on 253.5, 276, 300.5, 325.5 and 385 nm (average value), corresponding to characteristic Eu^{2+} electronic transitions from the $^8S_{7/2}$ ($4f^7$) ground state to the $4f^6$5d first excited configuration. Our results are in good agreement with those reported in the literature [53]. It is important to note that the peak localized around 325.5 nm remains without clear attribution, because the off-centered positions of the dopant induce a more complex splitting of the 5d levels than the simple model used by Mishra et al. [53]. As a consequence, all these observations allow us concluding that in combustion-derived BAM:Eu samples, divalent europium is mainly located in the three possible sites (BR, a-BR and mO). Moreover, focusing on individual band areas resulting from the refinement, it can be noticed that all the bands of reduced powder present higher areas than those of non-reduced powder.

Through magnetization and Mössbauer spectroscopy, we have previously demonstrated that the reduction treatment can enhance the percentage of divalent europium in blue phosphor by a factor two. Therefore, since optical performances of reduced powder were improved over the whole range of studied wavelengths, we can conclude that the reduction processing $Eu^{3+} \rightarrow Eu^{2+}$ is not selective in terms of crystallographic site: the Eu^{3+} ions located in the three available sites (BR, a-BR and mO) are reduced to Eu^{2+} ions.

The evolution of quantum yield with the excitation wavelength presented in Fig. 6 show that combustion-derived phosphors can be efficiently combined with a large variety of near-UV LED

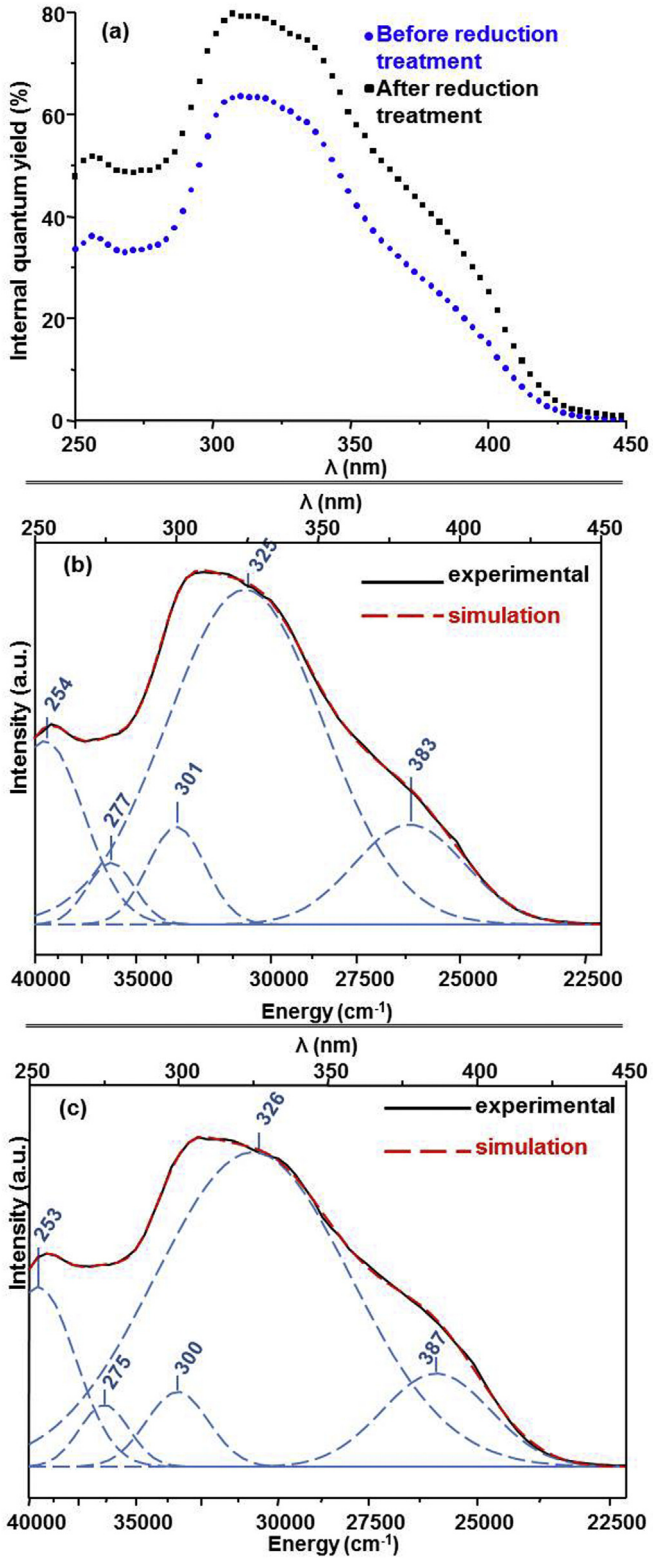

Fig. 6. Evolution of the room temperature photoluminescence quantum yield for BAM:Eu powders versus excitation wavelength (a); Gaussian fitted curve for BAM:Eu absolute photoluminescence quantum yields depending on the excitation wavelength (b) before and (c) after reduction.

emitting at wavelengths lying from 300 to 400 nm to lead blue luminescence. We have chosen to work with a 365 nm excitation wavelength, which corresponds to a conventional high-power commercial near-UV LED.

Fig. 7a displays the room-temperature emission spectra of both purified powders upon this 365 nm excitation. Emission intensity of reduced powder is significantly higher than that of non-reduced one, which is in good agreement with Fig. 6a and with the relative fractions of Eu^{2+} and Eu^{3+} determined by Mössbauer spectroscopy and magnetization. Furthermore, it can be noticed that, upon this excitation wavelength, no luminescence from Eu^{3+} (corresponding to $^5D_0$-^7F_J transitions) was observed in even for the powder containing 65% of Eu^{3+}. This phenomenon has already been observed in previous works [49] where it was ascribed to total quenching of Eu^{3+} emission due to energy transfer from Eu^{3+} to unwanted defects or impurities lying in their surroundings.

Each emission spectrum consists of a wide band centered at 450 nm. This broad band located in the blue region is due to Eu^{2+} ions transitions from the $4f^65d^1$ first excited configuration state to the $4f^7$ ($^8S_{7/2}$) ground state [54]. There is a slight asymmetry in both emission profiles, related to the three possible positions of europium ions in BAM matrix. Indeed, as previously seen, europium can occupy three sites (BR, a-BR and mO) with different symmetries.

As a consequence, in function of divalent europium localization, it will emit at different wavelengths [39,53,55]. Therefore, it is possible to decompose emission spectra in three Gaussians. Results are presented in Fig. 7b and c and Table 2 gathers the peak position and the area of each emission band but also tentative assignments of substituted sites. A comparison with the literature [39] is also given.

The fitting derives in Gaussian bands peaked around 443, 460 and 497 nm. Focusing on bands areas, both powders are characterized by a dominant emission located at 460 nm. Thus, the sites preferentially occupied by divalent europium are a-BR sites. These results are in agreement with those reported in the literature by Liu. et al. [39] who observed, for BAM:Eu samples prepared in a reducing atmosphere, that Eu^{3+} ions reduced in Eu^{2+} ions preferentially occupied a-BR sites. On the contrary, if the material was obtained under an oxidizing or neutral atmosphere the most important occupancy corresponded to BR sites. In our case, both powders were obtained under reducing conditions (during synthesis and during the reduction process) thus Eu^{2+} ions are preferentially located in a-BR sites.

Finally, the photoluminescence decay curves for the overall $4f^65d \rightarrow 4f^7$ transition of the Eu^{2+} ions in the purified BAM:Eu powders, collected upon a 365 nm excitation, were both fitted to a monoexponential function, $I = I_0 \exp(-t/\tau)$ (I_0 is the initial emission intensity, and τ is the lifetime of the emitting center, Eu^{2+}), as shown in Fig. 8.

The Eu^{2+} emission lifetimes derived from fits were determined to be approximately 1.28 and 1.14 μs before and after reduction (Fig. 8), respectively. These values are closed to that reported for the commercial BAM:Eu^{2+} [56], but differ notably from that of Eu^{2+} ions embedded in BAM synthesized by other processes than solid-state reaction [57] which are of about one hundred higher than that of our BAM:Eu^{2+} samples. Modifying the excitation wavelength in the vicinity of the Eu^{2+} excitation spectra leads exactly to the same decay shapes with the same lifetime values, indicating that no excitation selectivity can be reached. In spite of such a large discrepancy, the monoexponential character of our decays has been considered as a good indication of the homogeneous distribution of active ions in the MISCS derived materials. These decay times are short enough to be suitable in pc-WLEDs (<1 ms [58]).

When optical transitions are allowed (which is the case of $4f^65d^1 \rightarrow 4f^7$ ($^8S_{7/2}$) transition of Eu^{2+}), the emission cross-section depends inversely on luminescence decay time; a shortening of decay time with respect to the output quantum yield (Fig. 6a) is an indication that the emission cross-section is increased. Such an

Table 1
Summary of peak fitting on BAM:Eu powders photoluminescence quantum yields excitation spectra. The question mark (?) stands for a peak without clear attribution. (* BR: Beevers-Ross, a-BR: anti-Beevers-Ross, mO: middle-oxygen).

	Before reduction treatment			After reduction treatment			Lit.	Assignments*
	Energy (cm^{-1})	λ(nm)	Area(%)	Energy (cm^{-1})	λ(nm)	Area(%)	λ (nm)	
	39310	254	12.2	39506	253	14.4	253	BR
	36101	277	2.5	36364	275	3.4	276	a-BR/BR
	33264	301	4.8	33333	300	5.1	301	a-BR/mO
	30769	325	44.5	30675	326	66.2	337	?
	26110	383	9.5	25840	387	10.9	387	mO
$\sum$ areas	–	–	73.5	–	–	100		
R^2	0.99982			0.99974				

increase can be related to the rise in the concentration of Eu^{2+} emitting centers (which leads to the increase in the absorption cross-section), and also to the reduction of the non-radiative lifetime part from the excited states, τ_{NR}. An approximation of τ_{NR} can be estimated from the equation [59]: $(1-\eta)/\tau = 1/\tau_{NR}$ where τ is the fluorescence lifetime and η is the quantum efficiency at given excitation wavelength. Taking the experimental values of τ and the quantum efficiencies derived from Fig. 6a for excitation at 365 nm, the ratio between the τ_{NR} estimated before and after reduction is 0.74 (reduction of about 30%). The decrease in τ_{NR} consecutive to the reduction treatment indicates that non radiative recombination pathways are lowered after a reduction process.

3.5. Quantum efficiency and thermal stability of MISCS-derived BAM phosphors

Along with presenting the appropriate excitation profile, a phosphor intended to be used in high-power LEDs have to possess an important thermal stability since it has a significant impact on color rendering index and light output. On the other hand, it must also be characterized by good quantum efficiency. It is the reason why we studied temperature-dependent luminescence properties of MISCS-derived powders from RT till 170 °C (using conditions in high power near-UV LEDs) as well as their quantum yield before and after this thermal treatment. For comparison, the commercial BAM:Eu powder was also studied.

Fig. 9 shows emission spectra of commercial (Fig. 9a) and MISCS-derived reduced (Fig. 9b) BAM:Eu powders upon 365 nm excitation whereas the evolution of relative integrated emission area towards temperature is represented for both powders in Fig. 10, together with that of the non-reduced MISCS-derived BAM:Eu sample.

The emission intensity decreases and emission band shifts to shorter wavelengths as the temperature increases. The blue-shift of the main peak position can be explained in first approximation by the fact the host lattice expands as the temperature increases, which would cause a reduction in the crystal field splitting and leads to a higher energy emission. It is noteworthy to precise that emission spectra generally shift towards longer wavelength (red-shift) with increase in temperature according to configuration-coordinate model [60–62]. Blue-shift similar to that observed in Fig. 9 with the increase in temperature have already been obtained for some Eu^{2+}-doped compounds such as $(Sr,Ca)_2SiO_4:Eu^{2+}$ [63], $(Sr,Ba)_2Si_5N_8:Eu^{2+}$ and $(Sr,Ba)SiO_4:Eu^{2+}$ [61] or $K_4CaSi_3O_9:Eu^{2+}$ [64] while a red-shift was observed for example in $Sr_2SiO_4:Eu^{2+}$ [63]. From these reported results, it clearly appears that the shift is strongly correlated to the alkaline-earth cation sites (Ba, Sr or Ca) occupied by Eu^{2+}ions. On the basis that Eu^{2+} ions dwells in three inequivalent sites in BAM, these sites corresponding to different energy levels [53], the observed blue-shift is caused by thermally active phonon-assisted step from the excited states of low-energy site to the excited states of high-energy site (namely, from mO to BR sites in the case of BAM (see the study in the previous part). As temperature rises, the electrons population of upper vibrational levels of Eu^{2+} excited state becomes dominant under phonon assistance [20,22,30]. Thus, the radiative transition from this higher excited state entails the blue-shift of the maximum emission wavelength. The evolution of this maximum emission wavelength versus temperature is represented in details in Fig. S3. Commercial BAM is characterized by a much more significant blue-shift in emission (from 497 to 467 nm) than combustion derived powders (from 457 to 450 nm for reduced powder). It implies a better stability for color rendering index in WLEDs using MISCS-derived phosphors compared to those employing commercial BAM.

It can be seen from Fig. 10 that emission intensity decreases linearly with temperature for all samples. However, combustion-derived powders are less impacted by thermal quenching than the commercial one. Indeed, the PL emission area around 150 °C (423 K) drops to 70% and 88% of the initial values at RT for non-reduced and reduced combustion-derived powders respectively, while at the same temperature the emission intensity of the commercial BAM: Eu^{2+} phosphor decreases to 36% of its initial value, as shown in Fig. 10. The thermal quenching temperature ($T_{50\%}$) seems to be very high (highly superior to 200°C/473 K) for nanostructured phosphors whereas that of commercial BAM is around 120 °C(393 K). MISCS-derived BAM:Eu powders present a higher thermal stability than commercial BAM and the reduction step improves this feature.

This decrease in luminescence intensity observed in Figs. 9 and 10 is classical in such Eu^{2+}-doped phosphors [20,22,28,29]. It is generally ascribed to thermal quenching through the thermal excitation of the 5d electron to the conduction band states, using a configurational coordinate diagram [65] (see Fig. 11). With increasing temperature, phonon-electron interaction is enhanced. Through phonon interaction, excited Eu^{2+} ions are thermally activated from point A, the point of the lowest energy of excited state, to the crossing point C where the electronic states of the excited and ground states are intermixed. Then, they are thermally released from C to the lowest level of ground state. The energy ΔE necessary to excite the center from A to C is called the *thermal activation energy* of the material. The probability of this non-radiative transition (k_{NR}) from C to ground state increases with temperature, which explains the gradual decrease in emission efficiency when the temperature rises (Fig. 10) [65].

It has been suggested by Dorenbos [66] that the genuine thermal quenching mechanism of Eu^{2+} 5d–4f is the photoionization of the 5d electron to the upper conduction band. The energy barrier for thermal quenching depends on the energy difference between the lowest 5d state and the bottom of the conduction band. Dorenbos [66] gave two examples to discuss quenching behavior with type of alkaline-earth cation sites (Ba, Sr, or Ca) occupied by Eu^{2+}: (I) compounds where the bottom of the conduction band is formed

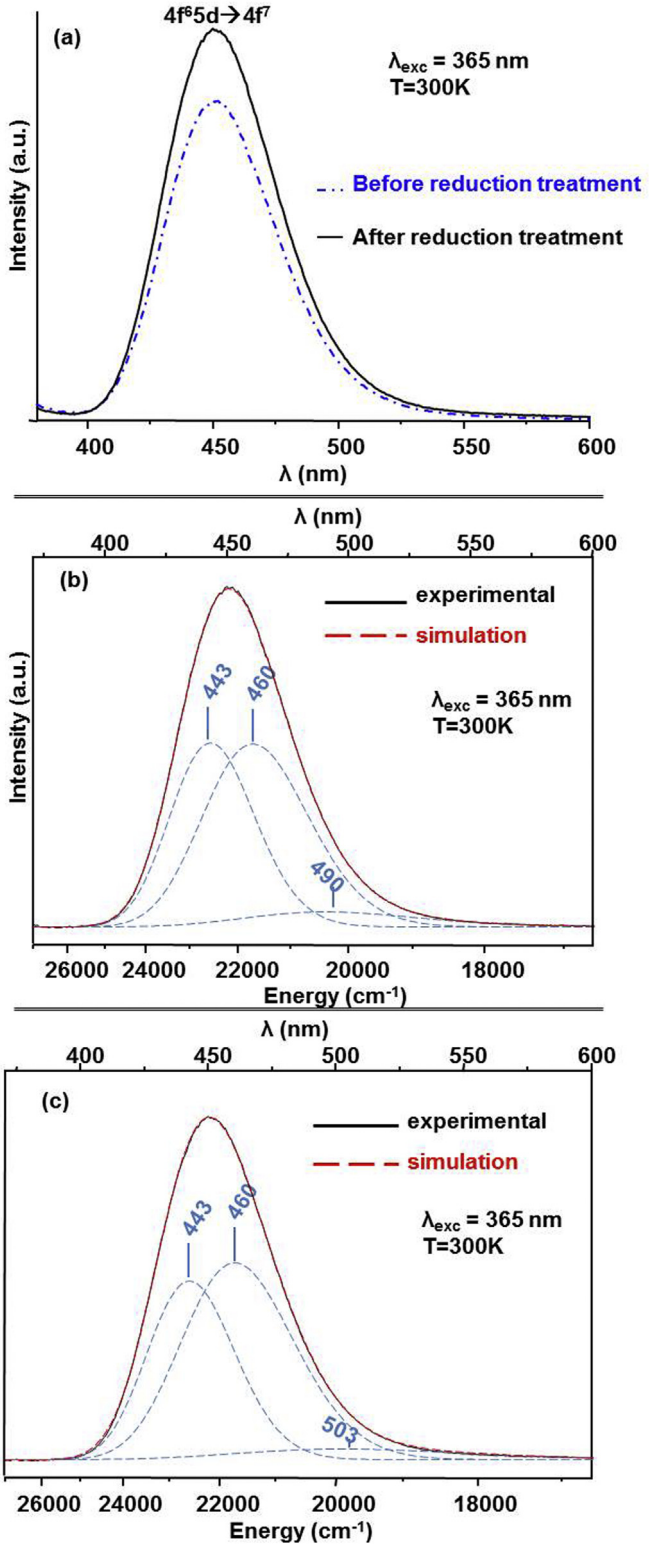

Fig. 7. Room-temperature emission spectra of BAM:Eu powders upon a 365 nm excitation (a); Gaussian fitted curve for BAM:Eu emission spectra upon a 365 nm excitation (b) before and (c) after reduction.

by the same cations as the ones replaced by Eu^{2+}, and (II) compounds where the bottom of the conduction band is dominated by cations other than the one replaced by Eu^{2+}. In type (I) compounds the activation energy for thermal quenching increases with smaller size of the alkaline-earth cation. In type (II) compounds the situation is reversed and the activation energy for thermal quenching decreases with smaller site of the alkaline-earth cation.

When this photoionization phenomenon is dominant, the emission intensity follows a modified Arrhenius equation (Eq. (2)):

$$\frac{I_T}{I_0} = \frac{1}{1 + c \cdot \exp\left(-\frac{\Delta E}{k_B T}\right)} \tag{2}$$

where I_0 is the initial emission intensity of the phosphor at room temperature, I_T is the emission of the phosphor at T, c is a constant, k_B is the Boltzmann constant (8.617×10^{-5} eV). If we try to plot the evolution of I_T/I_0 with temperature for both commercial and combustion-derived BAM:Eu phosphors, one can see in Fig. 12 that commercial BAM has a behavior corresponding to the previous formula with an activation energy around 0.291 eV. On the other hand, MISCS-derived reduced phosphor presents performances not consistent with this equation. This suggests that the decrease in luminescence for these phosphors involves mechanisms other than thermal quenching by photoionization.

Further investigations should be necessary to well identify the mechanisms coming into play but our first guess will be related to trapping centers and defects. Indeed, it has been demonstrated through thermoluminescence (TL) analysis that BAM lattice is characterized by two kind of traps levels, shallow and deep traps [67]. Reported results indicate that shallow traps are clearly related to oxygen vacancies. They do not have a negative influence on performances (efficiency and degradation) of BAM as a lighting phosphor. The luminescence efficiency and stability are strongly influenced by the formation of Eu^{3+} and a deeper trap during annealing in air. Subsequent annealing in a reducing atmosphere restores the original properties: the density of shallow traps decreases and the deep traps does not show up. Moreover, shallow traps structure is independent of excitation energy while deep trap TL signature is only observed at low energy excitation ($\lambda > 180$ nm).

On the other hand, Wang et al. [68] have related the higher stability of microwave-assisted sintered BAM (compared to solid-state derived one) to the intrinsic and extrinsic defects linked to the synthesis procedure. These deep traps and defects can act as electron traps and thus have a significant role in temperature dependence of phosphors. They can induce reversible changes in luminous output upon the UV radiation. Then electrons escaping to the conduction band of BAM:Eu by thermal activation can be captured by trapping centers. The ionization of Eu^{2+} results in a decrease in emission intensity but it is a reversible phenomenon. When the temperature decreases and the excitation light is cut off the trapped electrons can be released and recombine with the ionized Eu^{2+}. The emission intensity can then revert back to its initial value. Furthermore, it can be seen in Fig. 9a that commercial BAM is characterized by a broader emission band. This is certainly linked to another distribution of emitting centers in sites afore described: mO sites could notably be more occupied in commercial BAM than in combustion-derived powders. It is consistent with previous studies [39,52] that have shown a dependence of sites occupancy on the synthesis conditions of BAM:Eu. This discrepancy in the occupancy repartition of Eu^{2+} in the three crystallographic available sites could also be partly responsible for the differences in thermal behavior of the two kinds of BAM powders since they undergo thermal quenching in different ways.

To be sure that our MISCS-derived phosphors are suitable to be applied in solid-state lighting, we also continuously recorded emission spectra under 365 nm LED excitation at 170 °C during several hours. Main results are gathered in Fig. 13.

The inset shows the emission intensity drops to 92% of its initial

Table 2
Summary of peak fitting on BAM:Eu powders emission spectra upon a 365 nm excitation (*(BR: Beevers-Ross, a-BR: anti-Beevers-Ross, mO: middle-oxygen).

	Before reduction treatment			After reduction treatment			Lit.	Assignments*
	Energy (cm^{-1})	λ (nm)	Area(%)	Energy (cm^{-1})	λ (nm)	Area(%)	λ (nm)	
	22577	443	35.2	22596	443	41.0	441	BR
	21724	460	40.6	21723	460	53.8	461	a-BR
	20398	490	4.8	19899	503	5.2	497	mO
∑ areas	–	–	80.6	–	–	100		
R^2	0.99995			0.99994				

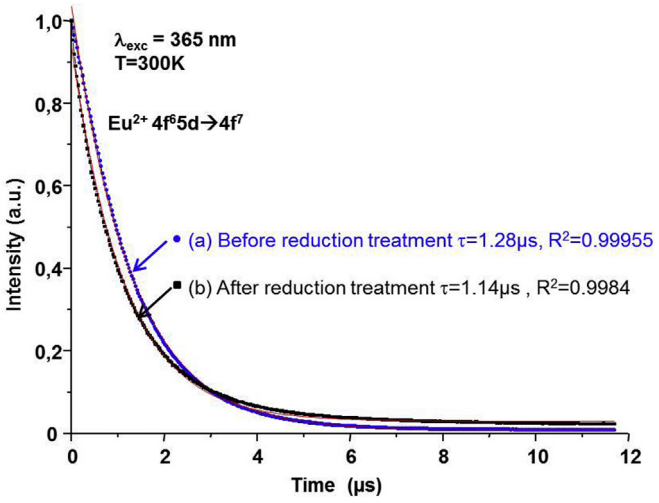

Fig. 8. Decay curves of Eu^{2+} ions $4f^65d^1 \rightarrow 4f^7$ ($^8S_{7/2}$) (transition in BAM purified powders (a) before and (b) after reduction collected upon a 365 nm excitation at 300 K.

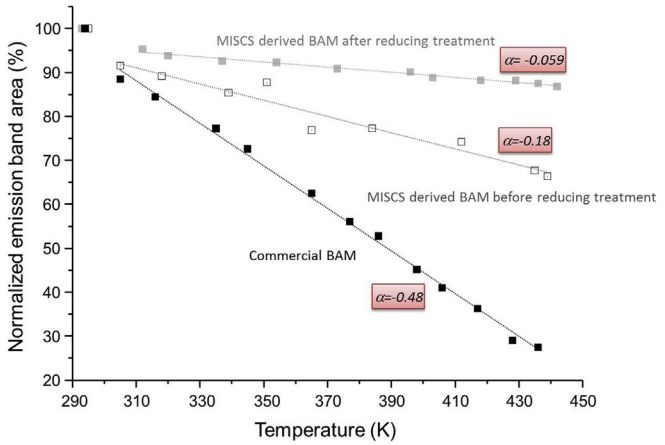

Fig. 10. Evolution with temperature of the normalized emission band area of BAM:Eu powders upon a 365 nm LED excitation: commercial and MISCS-derived BAM:Eu powders. Dot lines represent linear fits of the evolutions with corresponding slopes α.

value after 15 h of irradiation at 170 °C whereas the emission band is slightly red-shifted during the first 3 h then it remains almost stable around 455 nm. It can be concluded that luminescence properties of our combustion-derived BAM:Eu powders are highly stable under operating conditions characteristic of near-UV LED based lighting devices.

Finally, absolute quantum yields of reduced MISCS-derived BAM:Eu have been measured versus excitation wavelengths and compared to commercial BAM:Eu. Results are gathered in Fig. 14. Spectra of combustion-derived powders are similar to those shown in Fig. 6a with a broad band lying from 300 to 420 nm due to the multiple sites for Eu^{2+} (see RT photoluminescence study). Commercial BAM exhibits an absolute quantum yield superior to that of combustion-derived powders whatever the excitation wavelength. For example, for a 365 nm-excitation, commercial BAM shows an external quantum efficiency around 65%, which is consistent with previous studies [22], whereas the reduced MISCS-derived powder exhibits an absolute QY of 33%. This difference can be ascribed to a higher crystallinity for commercial BAM which could be the result of a higher heating temperature during the synthesis process. Hence, their optical features are very interesting for use in solid-state lighting subject to the improvement of their absolute quantum yield.

After being exposed for 15 h to a temperature of 170 °C under a 365 nm-excitation, samples are called “heated”. From Fig. 14

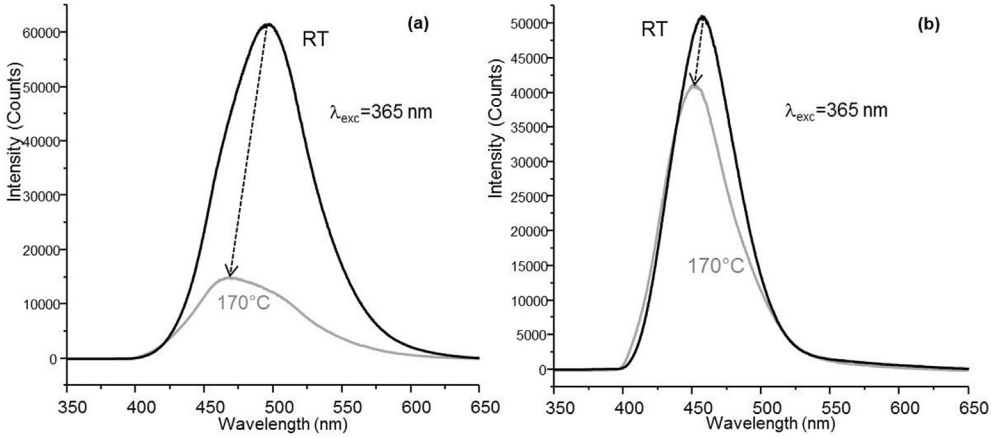

Fig. 9. Emission spectra of BAM:Eu powders upon a 365 nm LED excitation at room temperature and at 170 °C: commercial BAM (a) and MISCS-derived BAM (b).

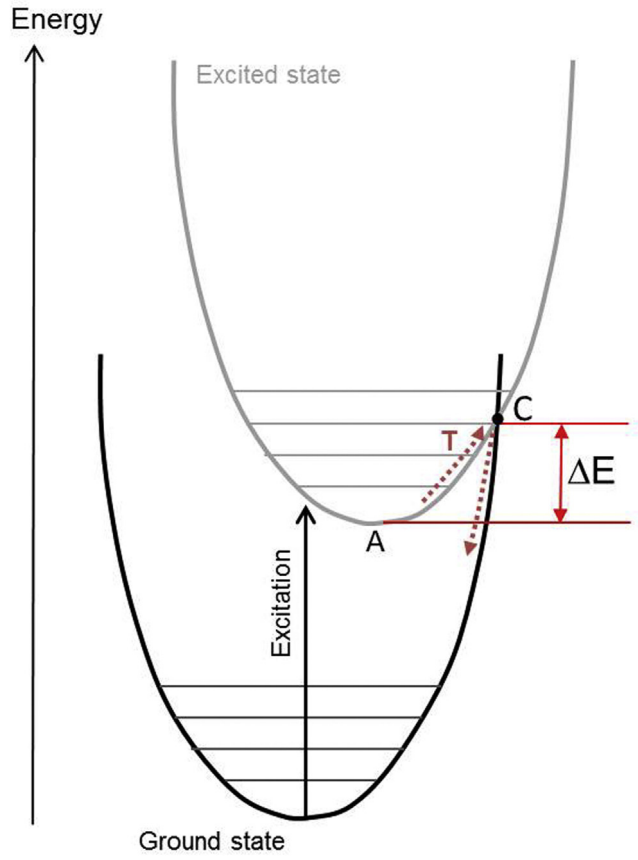

Fig. 11. Configurational coordinate diagram illustrating quenching of the luminescence at higher temperatures by thermally stimulated cross-over from the excited state to the ground state.

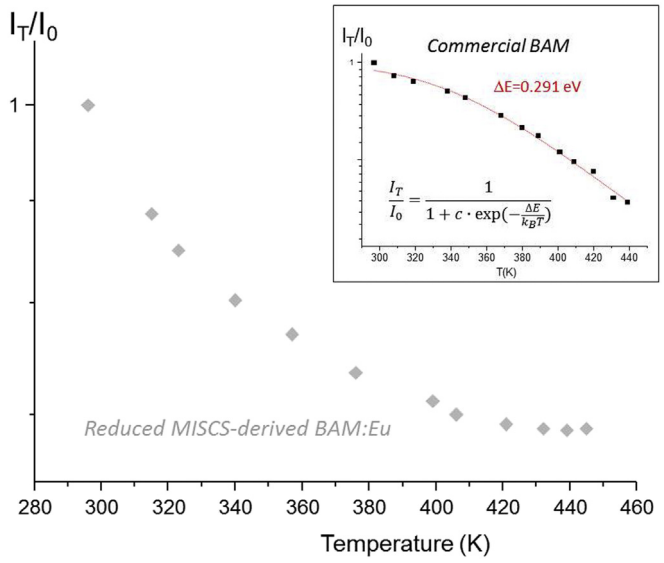

Fig. 12. Evolution with temperature of the ratio I_T/I_0 for combustion-derived reduced powder and (inset) commercial BAM. For this latter, a fit using Eq. (1) has been used to determine ΔE.

(empty squares and diamonds compared to filled symbols), it can be clearly seen that commercial BAM:Eu have truly undergone a thermal degradation with significant irreversible effects (drops to

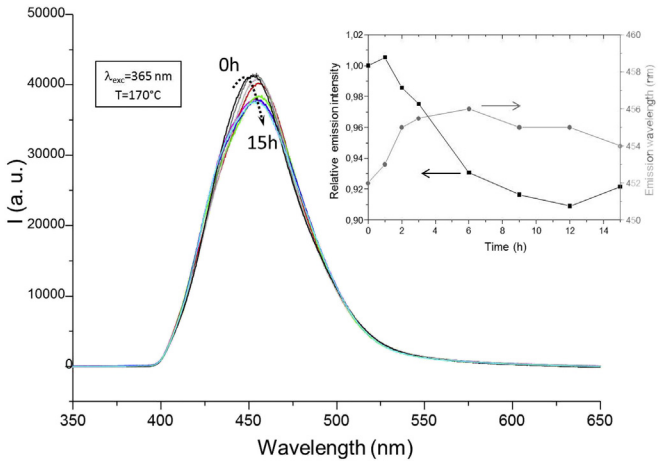

Fig. 13. Evolution of the emission spectra of reduced MISCS-derived BAM:Eu powder with time (λ_{exc} = 365 nm and T = 170 °C).

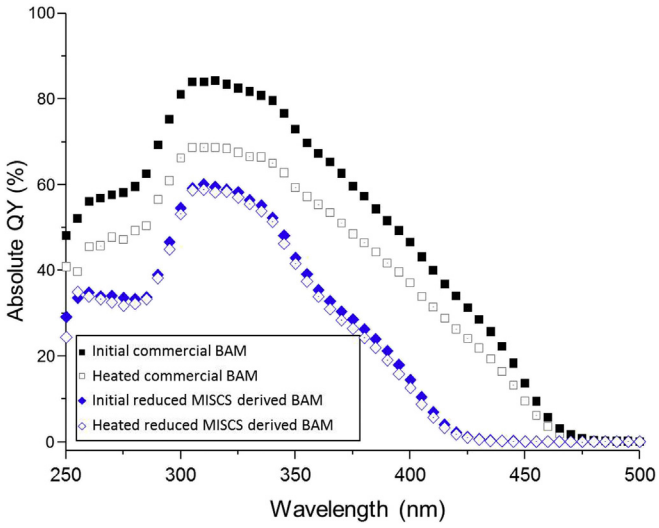

Fig. 14. Evolution of the room temperature absolute photoluminescence quantum yield versus excitation wavelength for combustion-derived and commercial BAM:Eu before ("initial") and after ("heated") 15 h at 170 °C under 365 nm.

82% of its initial value at 365 nm) whereas MISCS-derived phosphor has almost recovered the quantum yields of the initial powder (drops only to 94% of its initial value at 365 nm). This is another strong evidence that at least a part of thermal quenching mechanisms are different between the two kinds of powders. It can be assumed that the irreversible effects for BAM commercial correspond to an oxidation of Eu^{2+}, even if we could neither make further Mössbauer experiments nor see emission lines from Eu^{3+} ions in emission spectra [49]. The reversibility of the thermal quenching of MISCS-derived BAM:Eu powder is consistent with a mechanism involving trapping centers, as described above.

4. Conclusions

$BaMgAl_{10}O_{17}:Eu^{2+}$ blue phosphor has been synthesized through a simple and rapid microwave-assisted combustion procedure. This method allows obtaining well-crystallized, plate-like shape nanostructured and pure BAM phase after two purification steps: the first one is an acid-washing, leading to $BaAl_2O_4$ phase removal still present at the end of the synthesis, whereas the second one

consisted in a post-heating treatment in a reducing atmosphere in order to enhance the quantity of Eu^{2+} responsible for the desired luminescence properties. An original study by magnetization and Mössbauer spectroscopy allowed us determining the relative fractions of Eu^{2+}/Eu^{3+} in the samples: the reduction treatment results in an increase in the percentage of Eu^{2+} by a factor of two, leading to a gain in the luminescence efficiency, as demonstrated through the detailed optical study. The luminescence investigations enable us to determine the europium localization in BAM matrix: the sites preferentially occupied by divalent europium are anti-Beevers-Ross ones. Furthermore, compared to commercial BAM, MISCS-derived powders, notably those obtained after the reduction treatment, show a higher thermal stability in using conditions of high power LEDs, ensuring long-lasting suitable photometric parameters for UV-LED based devices. In addition, they are less degraded after 15 h at 170 °C than commercial BAM. To conclude, even if they exhibit an absolute QY significantly inferior to that of commercial BAM, their efficiency can be suitably enhanced working on synthesis process as well as using an inert shell. Our phosphors revealed to be promising candidates for solid-state lighting if their optical performances are improved.

Acknowledgements

The authors would like to thank Anne-Marie Gélinaud (2MATech, Aubière, France) for her help in acquiring the SEM pictures.

Appendix A. Supplementary data

Supplementary data related to this article can be found at http://dx.doi.org/10.1016/j.optmat.2016.12.031.

References

[1] S.R. Jain, K.C. Adiga, V.R. Pai Verneker, Combust. Flame 40 (1981) 71–79.
[2] S. Ye, F. Xiao, Y.X. Pan, Y.Y. Ma, Q.Y. Zhang, Mater. Sci. Eng. R 71 (2010) 1–34.
[3] L. Chen, C.-C. Lin, C.-W. Yeh, R.-S. Liu, Materials 3 (2010) 2172–2195.
[4] X. Ye, L. Qi, Nano Today 6 (2011) 608–631.
[5] J.Y. Tsao, M.H. Crawford, M.E. Coltrin, A.J. Fischer, D.D. Koleske, G.S. Subramania, G.T. Wang, J.J. Wierer, R.F. Karlicek, Adv. Opt. Mater. 2 (2014) 809–836.
[6] S. Yang, Y. Lei, Nanoscale 3 (2011) 2768–2782.
[7] P.F. Smet, A.B. Parmentier, D. Poelman, J. Electrochem. Soc. 158 (2011) R37–R54.
[8] G. Li, Y. Tian, Y. Zhao, J. Lin, Chem. Soc. Rev. 44 (2015) 8688–8713.
[9] J.K. Han, J.I. Choi, A. Piquette, M. Hannah, M. Anc, M. Galvez, J.B. Talbot, J. McKittrick, ECS J. Solid State Sci. Technol. 2 (2013) R3138–R3147.
[10] Y. Tian, J. Solid State Light. 1 (2014) 1–15.
[11] J. McKittrick, L.E. Shea-Rohwer, J. Am. Ceram. Soc. 97 (2014) 1327–1352.
[12] C.C. Lin, R.-S. Liu, J. Phys. Chem. Lett. 2 (2011) 1268–1277.
[13] C.R. Ronda, J. Lumin. 72–74 (1997) 49–54.
[14] C.-H. Kim, I.-E. Kwon, C.-H. Park, Y.-J. Hwang, H.-S. Bae, B.-Y. Yu, C.-H. Pyun, G.-Y. Hong, J. Alloys Compd. 311 (2000) 33–39.
[15] K. Toda, J. Alloys Compd. 408–412 (2006) 665–668.
[16] K. Takashi, F. Yoshiko, H. Tetsuo, K. Youji, N. Kimihiko, O. Koutoku, Jpn. J. Appl. Phys. 53 (2014) 05FK03.
[17] A. Lacanilao, G. Wallez, L. Mazerolles, P. Dubot, L. Binet, B. Pavageau, L. Servant, V. Buissette, T. Le Mercier, Solid State Ionics 253 (2013) 32–38.
[18] Q. Zhu, M. Xiong, J.-G. Li, W. Liu, Z. Wang, X. Li, X. Sun, RSC Adv. 5 (2015) 36122–36128.
[19] Y.-F. Wang, Q.-Q. Zhu, L.-Y. Hao, X. Xu, R.-J. Xie, S. Agathopoulos, J. Am. Ceram. Soc. 96 (2013) 2562–2569.
[20] Z.-C. Wu, H.-H. Fu, J. Liu, S.-P. Kuang, M.-M. Wu, J.-G. Xu, X.-J. Kuang, RSC Adv. 5 (2015) 42714–42720.
[21] Z.-C. Wu, S. Wang, J. Liu, J.-H. Yin, S.-P. Kuang, J. Alloys Compd. 644 (2015) 274–279.
[22] G.-y. Lee, J.Y. Han, W.B. Im, S.H. Cheong, D.Y. Jeon, Inorg. Chem. 51 (2012) 10688–10694.
[23] Q. Shao, H. Lin, Y. Dong, Y. Fu, C. Liang, J. He, J. Jiang, J. Solid State Chem. 225 (2015) 72–77.
[24] W. Xiao, X. Zhang, Z. Hao, G.-H. Pan, Y. Luo, L. Zhang, J. Zhang, Inorg. Chem. 54 (2015) 3189–3195.
[25] Y. Zhang, Z. Xia, W. Wu, J. Am. Ceram. Soc. 96 (2013) 1043–1046.
[26] S. Zhang, X. Wu, Y. Huang, H.J. Seo, Int. J. Appl. Ceram. Technol. 8 (2011) 734–740.
[27] Z. Xia, S. Miao, M.S. Molokeev, M. Chen, Q. Liu, J. Mater. Chem. C 4 (2016) 1336–1344.
[28] L. Wang, H. Zhang, X.-J. Wang, B. Dierre, T. Suehiro, T. Takeda, N. Hirosaki, R.-J. Xie, Phys. Chem. Chem. Phys. 17 (2015) 15797–15804.
[29] W. Lv, Y. Jia, Q. Zhao, W. Lü, M. Jiao, B. Shao, H. You, J. Phys. Chem. B 118 (2014) 4649–4655.
[30] K.-T. Hsu, P.-C. Lin, I.V.B. Maggay, C.-H. Huang, W.-R. Liu, S.-M. Chang, Mater. Express 5 (2015) 255–260.
[31] Z. Chen, Y. Yan, J. Liu, Y. Yin, H. Wen, J. Zao, D. Liu, H. Tian, C. Zhang, S. Li, J. Alloys Compd. 473 (2009) L13–L16.
[32] N. Pradal, A. Potdevin, G. Chadeyron, R. Mahiou, Mater. Res. Bull. 46 (2011) 563–568.
[33] Y. Kim, S. Kang, Appl. Phys. B 98 (2010) 429–434.
[34] Z.H. Zhang, Y.H. Wang, X.X. Li, Y.K. Du, W.J. Liu, J. Lumin. 122–123 (2007) 1003–1005.
[35] B.V. Ratnam, M. Jayasimhadri, G. Bhaskar Kumar, K. Jang, S.S. Kim, Y.I. Lee, J.M. Lim, D.S. Shin, T.K. Song, J. Alloys Compd. 564 (2013) 100–104.
[36] A. Potdevin, N. Pradal, M.-L. François, G. Chadeyron, D. Boyer, R. Mahiou, Microwave-induced combustion synthesis of luminescent aluminate powders, in: D.V. Shatokha (Ed.), Sintering - Methods and Products, InTech, 2012, pp. 189–212.
[37] Z. Chen, Y. Yan, Phys. B 392 (2007) 1–6.
[38] N. Pradal, G. Chadeyron, S. Therias, A. Potdevin, C.V. Santilli, R. Mahiou, Dalton Trans. 43 (2014) 1072–1081.
[39] B. Liu, Y. Wang, J. Zhou, F. Zhang, Z. Wang, J. Appl. Phys. 106 (2009), 053102–053102-053105.
[40] Z. Zhang, J. Feng, Z. Huang, Particuology 8 (2010) 473–476.
[41] Y.-I. Kim, S.-O. Kang, J.-S. Lee, M.-J. Jung, K.H. Kim, J. Mater. Sci. Lett. 21 (2002) 219–222.
[42] K.-B. Kim, Y.-I. Kim, H.-G. Chun, T.-Y. Cho, J.-S. Jung, J.-G. Kang, Chem. Mater. 14 (2002) 5045–5052.
[43] P. Boutinaud, E. Cavalli, M. Bettinelli, J. Phys. Condens. Matter 19 (2007) 386230.
[44] B.D. Cullity, Elements of X-Ray Diffraction, second ed., Addison-Wesley, Reading, Massachussets, 1978.
[45] X. Tian, Z. Weidong, C. Xiangzhong, Z. Chunlei, T. Xiaoming, H. Xiaowei, J. Rare Earth 24 (2006) 141–144.
[46] S. Arajs, R.V. Colvin, J. Appl. Phys. 35 (1964) 1181.
[47] F. Clabau, A. Garcia, P. Bonville, D. Gonbeau, T. Le Mercier, P. Deniard, S. Jobic, J. Solid State Chem. 181 (2008) 1456–1461.
[48] P. Boolchand, K.C. Mishra, M. Raukas, A. Ellens, P.C. Schmidt, Phys. Rev. B 66 (2002) 134429.
[49] K.C. Mishra, M. Raukas, G. Marking, P. Chen, P. Boolchand, J. Electrochem. Soc. 152 (2005) H183–H190.
[50] H. Toyoshima, S. Watanabe, K. Ogasawara, H. Yoshida, J. Lumin. 122–123 (2007) 104–106.
[51] R. Turos-Matysiak, M. Grinberg, J.W. Wang, W.M. Yen, R.S. Meltzer, J. Lumin. 122–123 (2007) 107–109.
[52] J. Lambert, G. Wallez, M. Quarton, T. Le Mercier, W. van Beek, J. Lumin. 128 (2008) 366–372.
[53] K.C. Mishra, M. Raukas, A. Ellens, K.H. Johnson, J. Lumin. 96 (2002) 95–105.
[54] Z. Chen, Y. Yan, Phys. B 392 (2007) 1–6.
[55] A. Ellens, F. Zwaschka, F. Kummer, A. Meijerink, M. Raukas, K. Mishra, J. Lumin. 93 (2001) 147–153.
[56] G. Bizarri, B. Moine, J. Lumin. 115 (2005) 53–61.
[57] R. Shanker, A.F. Khan, R. Kumar, H. Chander, V. Shanker, S. Chawla, J. Lumin. 143 (2013) 173–180.
[58] H. Winkler, Q.T. Vinh, T.Q. Khanh, A. Benker, C. Bois, R. Petry, A. Zych, LED Components – Principles of radiation generation and packaging, in: LED Lighting, Wiley-VCH Verlag GmbH & Co. KGaA, 2014, pp. 49–132.
[59] S. Singh, R.G. Smith, L.G. Van Uitert, Phys. Rev. B 10 (1974) 2566–2572.
[60] T. Tsuboi, P. Silfsten, J. Phys. Condens. Matter 3 (1991) 9163.
[61] L. Chen, C.-C. Lin, C.-W. Yeh, R.-S. Liu, Materials 3 (2010) 2172–2195.
[62] C.-H. Park, Y.-N. Choi, J. Solid State Chem. 182 (2009) 1884–1888.
[63] J.S. Kim, Y.H. Park, S.M. Kim, J.C. Choi, H.L. Park, Solid State Commun. 133 (2005) 445–448.
[64] B. Yuan, X. Wang, T. Tsuboi, Y. Huang, H.J. Seo, J. Alloys Compd. 512 (2012) 144–148.
[65] S. Shionoya, Phosphor Handbook, CRC Press, Boca Raton, 1998.
[66] P. Dorenbos, J. Phys. Condens. Matter 17 (2005) 8103.
[67] T. Jüstel, H. Lade, W. Mayr, A. Meijerink, D.U. Wiechert, J. Lumin. 101 (2003) 195–210.
[68] Y.-F. Wang, L. Liu, R.-J. Xie, Q. Huang, ECS J. Solid State Sci. Technol. 2 (2013) R196–R200.